Adsorption 11: 235–244, 2005

Sorption Kinetics and Intracrystalline Diffusion of Methanol in Ferrierite: An Example of Disguised Kinetics

P. KORTUNOV, C. CHMELIK AND J. KÄRGER
Universität Leipzig, Fakultät für Physik und Geowissenschaften, Linnéstr. 5, D-04103 Leipzig, Germany

R.A. RAKOCZY
Universität Stuttgart, Institut für Technische Chemie, Pfaffenwaldring 55, D-70550 Stuttgart, Germany

D.M. RUTHVEN
University of Maine, Department of Chem. Engineering, 5737 Jenness Hall Orono, Maine 04469-5737, USA

Y. TRAA
Universität Stuttgart, Institut für Technische Chemie, Pfaffenwaldring 55, D-70550 Stuttgart, Germany

S. VASENKOV
Universität Leipzig, Fakultät für Physik und Geowissenschaften, Linnéstr. 5, D-04103 Leipzig, Germany

J. WEITKAMP
Universität Stuttgart, Institut für Technische Chemie, Pfaffenwaldring 55, D-70550 Stuttgart, Germany

Abstract. Sorption kinetics of methanol in large crystals of ferrierite have been studied in detail by interference microscopy (IFM) and infra-red microscopy (IRM). The IFM measurements yield the transient concentration profiles, thus providing a direct measurement of both the surface resistance to mass transfer and the internal diffusion resistance. It is shown that, for this system, the uptake rate is controlled by the combined effects of surface resistance and diffusion through the 8-ring channels (in the y-direction). Transport through the 10-ring channels (in the z-direction) appears to be blocked by surface resistance. Although the overall uptake curves conform well to the "root t law" the diffusivity values derived from the uptake curves vary widely depending on the assumed direction of diffusion. Even if the correct direction of diffusion is assumed, the diffusivity values derived from the uptake curves are seriously in error as a result of the intrusion of surface resistance. The existence of transport resistances at the crystal surface is clearly apparent from the transient concentration profiles but is not obvious from the uptake curves.

Keywords: diffusion, zeolite, concentration profiles, surface barrier, interference microscopy, IR microscopy

Introduction

Professor Wolfgang Schirmer is one of the true pioneers of zeolite research. Under his leadership the Institute of Physical Chemistry of the Academy of Sciences of the German Democratic Republic achieved world-wide recognition as one of the major centers of research in fundamental zeolite science and the technical application of zeolites as catalysts and selective adsorbents. The numerous publications of his research

group are still widely cited. Two of the authors of the present paper (Jörg Kärger and Douglas Ruthven) owe a special debt of gratitude to Professor Schirmer as it was he who introduced them (in May 1973), leading to a productive research collaboration and a highly valued personal friendship spanning more than thirty years.

Several of Professor Schirmer's earlier papers (see for example Schirmer et al., 1968) dealt with the kinetics of sorption in zeolite adsorbents which is the subject of the present research. In earlier studies it was generally assumed that the diffusion of the sorbate through the small intracrystalline pores of the zeolite is the rate limiting process that controls the sorption kinetics. The importance of extracrystalline resistances to heat and mass transfer was recognized only in the late 1970s in response to PFG NMR diffusion measurements carried out at the University of Leipzig under Professor Pfeifer's direction, which showed clearly that, at least for some systems such as water or light paraffins in 5A and 13X, intracrystalline diffusion is much faster than is suggested by the overall sorption kinetics (Kärger et al., 1976; Kärger and Caro, 1977).

This observation led to the development and application of several new experimental techniques, such as frequency response and ZLC, aimed at eliminating or minimizing the intrusion of extracrystalline resistances (Yasuda, 1982; van den Begin and Rees, 1989; Eic and Ruthven, 1988). More recently two important "meso/microscopic" techniques which measure sorption and diffusion at the scale of the individual zeolite crystal have been developed: infra-red absorption (Hermann et al., 1995) and interference microscopy (Kärger et al., 2000).

Experimental

Measurements were made by both infra-red (IR) absorption and interference microscopy. Over a wide range of wave numbers the zeolite framework is transparent to IR radiation. The absorbance at a properly selected waveband therefore provides a direct measure of the molecular density of the adsorbed phase within the field of view, averaged over the path length of the beam through the crystal. This technique was first applied to individual zeolites by Hermann, Niessen and Karge to study the uptake of n-hexane by ZSM-5 (Hermann et al., 1995). The relatively long wavelength, however, means that the resolution is of the order of several micrometers, so the method can be used to measure the overall uptake in an individual crystal (or in a part of a crystal) but it does not have sufficient resolution to measure the intracrystalline sorbate concentration profile except in very large crystals.

In contrast, the interference microscopy technique, introduced by Kärger et al. which depends on measuring changes in the optical path length due to the presence of sorbate within the crystal, has a much higher spatial resolution (0.5 μm) (Kärger et al., 2000). This is sufficient to allow the accurate measurement of the transient concentration profiles in zeolite crystals larger than about 10 μm. The measurements yield the *average* sorbate concentration in the direction of the light beam. If the concentration is uniform in this direction the calculation of the profile is straightforward, but if there is a concentration profile in this direction (as is the situation with an isotropic crystal) the extraction of the concentration profiles from the measured changes in optical path length becomes much more complicated (Geier et al., 2001).

The experimental set-up consists of a vacuum system and a JENAPOL interference microscope (Carl Zeiss GmbH) with an interferometer of Mach-Zehnder type for interference microscopy measurements, and of the IR microscope UMA 500 attached to the FTIR spectrometer FTS 6000 (Digilab), which is equipped with a motorized stage, for IR microscopy measurements. Interference patterns were recorded during adsorption and desorption by a CCD camera (XC-77CE, Sony).

The sample of pure silicon ferrierite which was studied was synthesized by Racokzy (Stuttgart) and is practically free of OH groups (no bands in the IR spectrum). The crystals size is about $200 \times 50 \times 10\,\mu m^3$. The N_2 sorption capacity was found to be $129.4\,cm^3 \cdot STP/g$.

For the measurements the calcined zeolite sample was introduced into a specially made optical or IR cell connected to a vacuum system. Prior to the measurements, the sample was activated by keeping it under high vacuum at elevated temperature (typically at around 200°C) for over 12 h. To exclude the influence of organic residuals the experiments were repeated after a second calcination step (450°C for about 4 h).

The measurements of the concentration integrals were all performed at room temperature with one selected zeolite crystal. Adsorption or desorption was initiated by appropriate step changes of the methanol pressure in the surrounding gas phase. The equilibration time for the system pressure is less than 1 s compared with sorption times of several thousand seconds. Since

no inert was present there can be no gas side resistance to mass transfer.

Theoretical

The experimental data are interpreted according to standard kinetic models for diffusion-controlled systems (Crank, 1956). For a system in which the controlling resistance is diffusion through the surface layer the uptake curve following a step change in concentration (or ambient sorbate pressure) is given by:

$$\frac{m_t - m_0}{m_\infty - m_0} = 1 - \exp(-\alpha a t) \tag{1}$$

where m_∞ is the final loading (at equilibrium with the ambient gas), m_t is the sorbate loading at time t, m_0 is the initial loading before the step change in concentration, α is the mass transfer rate coefficient and a is the ratio of the external surface area to volume. For such a system a plot of $\ln(1-(m_t-m_0)/(m_\infty-m_0))$ vs. time (t) should yield a straight line through the origin with slope -αa, allowing a simple test of the model and a straightforward extraction of the mass transfer rate coefficient (α). Note that Eq. (1) is applicable regardless of the dimensionality of the adsorbent pore system and applies equally for adsorption and desorption provided that α is independent of loading over the relevant range.

If the sorption rate is controlled by internal diffusion (diffusivity D) the corresponding expressions for the uptake curve are:

Sphere:

$$\frac{m_t - m_0}{m_\infty - m_0} = 1 - \frac{6}{\pi^2}\sum_{n=1}^{\infty}\frac{1}{n^2}\exp(-n^2\pi^2 Dt/R^2) \tag{2}$$

Slab (one dimensional system) :

$$\frac{m_t - m_0}{m_\infty - m_0} = 1 - \frac{8}{\pi^2}\sum_{n=0}^{\infty}\frac{\exp[-(2n+1^2\pi^2 Dt/4\ell^2]}{(2n+1)^2} \tag{3}$$

where R is the radius of the sphere and l the half-thickness of the parallel sided slab. Up to about 50% uptake both these expressions are well approximated by the limiting form for short times:

$$\frac{m_t - m_0}{m_\infty - m_0} \approx 2a\sqrt{\frac{Dt}{\pi}} \tag{4}$$

Plots of $\ln(1 - (m_t - m_0)/(m_\infty - m_0))$ vs. t and $(m_t - m_0)/(m_\infty - m_0)$ vs.$\sqrt{t}$ thus provide a simple way to distinguish between surface-controlled and internal diffusion controlled processes.

It is worth noting that a sorption rate measurement can yield only the diffusional time constant (R^2/D or l^2/D). To estimate the diffusivity requires either knowledge or an assumption concerning the dimensionality and extension of the pore system.

For a unidimensional system in which both the surface and internal resistances are of similar magnitude the uptake curve is given by:

$$\frac{m_t - m_0}{m_\infty - m_0} = 1 - \sum_{n=1}^{\infty}\frac{2L^2\exp\left(-\beta_n^2 Dt/\ell^2\right)}{\beta_n^2\left(\beta_n^2 + L^2 + L\right)} \tag{5}$$

where $L \equiv \frac{\ell\alpha}{D} = \beta_n \tan\beta_n$. For $L \to 0$ this expression reduces to Eq. (1) while for $L \to \infty$ it reduces to Eq. (3). The internal concentration profile is given by:

$$\frac{q - q_0}{q_\infty - q_0} = 1 - \sum_{n=1}^{\infty}\frac{2L\cos(\beta_n y/\ell)\exp\left(-\beta_n^2 Dt/\ell^2\right)}{\left(\beta_n^2 + L^2 + L\right)\cos\beta_n} \tag{6}$$

where q_∞ is the final concentration (at equilibrium with the ambient gas), q is the sorbate concentration in position y at time t and q_0 is the initial concentration (i.e. at time $t = 0$) before the step change in concentration.

Results and Discussion

The shape and dimensions of the ferrierite crystal are shown in Figure 1 together with two-dimensional (2D) concentration profiles and concentration profiles in the y-direction (near the crystal edge, $z = 2\,\mu$m) and in the z-direction (for middle part of crystal, $y = 25\,\mu$m), measured by interference microscopy at various times. Ferrierite has a two-dimensional (interconnected) pore system with 10-ring channels in the z-direction and 8-ring channels in the y-direction (Meier and Olson, 1992). There are no pores in the x-direction which is the direction of the light beam.

The shape of the concentration profiles is quite different from what would be expected for diffusion into a rectangular slab along the z-direction and, to our initial surprise, the final equilibrium intensity (for adsorption) shows a well defined maximum at the

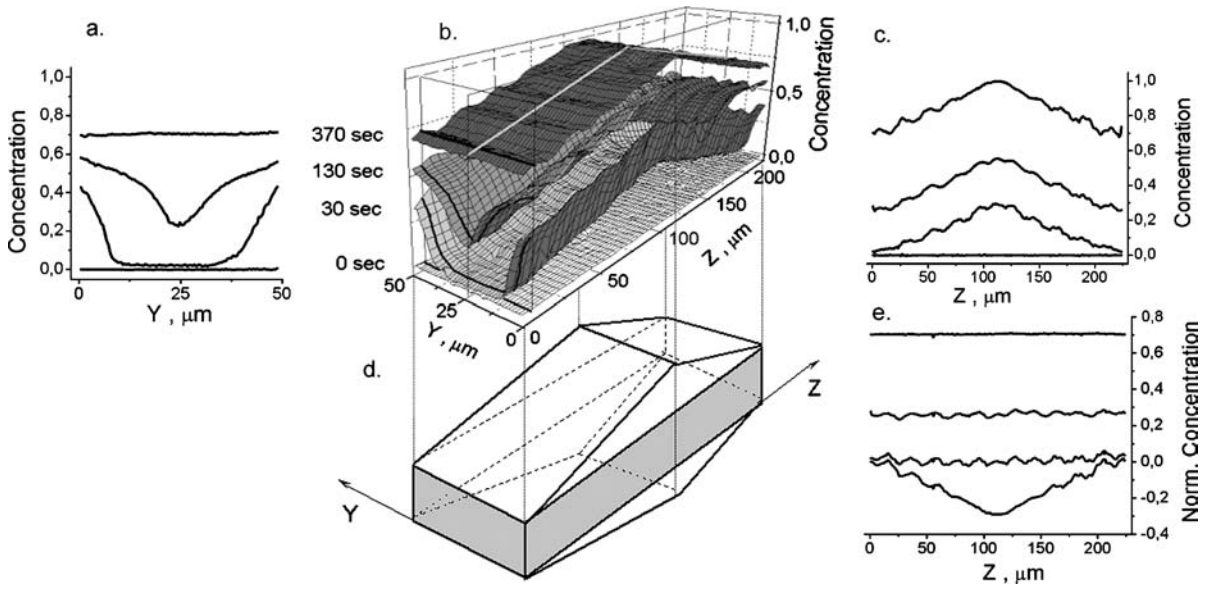

Figure 1. Shape and dimensions of the ferrierite crystal (d), 2D-concentration profiles for the entire crystal (b) and intensity profiles in the y-direction near the crystal edge, $z = 2\,\mu$m (a $\equiv$ fat black line in the profiles of Fig. 1b) and z-direction in the middle part of the crystal, $y = 25\,\mu$m (c) measured by interference microscopy for pressure step $0 \rightarrow 80$ mbar. The normalized concentration profiles along z-direction derived by subtracting the "roof–like" profile are shown (e). Profiles shown in *a*, *b*, *c*, *e* were measured at the same times after the start of adsorption.

center of the crystal (Fig. 1(c)). After some thought we realized that this maximum may be simply a consequence of the crystal shape since the optical path is larger in the center of the crystal than at the edges (Fig. 1(d)). The profiles were therefore corrected by subtracting the final equilibrium intensity at each point (Fig. 1(e)). This procedure yielded profiles which, after a short initial transient, are essentially flat over the entire length of the crystal (Fig. 1(e)). Coupled with the observation that there is a well defined concentration gradient in the y-direction (Fig. 1(a)) this suggests that the "roof" sections of the crystal fills rapidly through the 10-ring channels in the z-direction (accounting for the initial transient) but the central cuboid portion of the crystal fills relatively slowly and only through the 8-ring channels in the y-direction. The 10-ring channels of the central cuboid portion of the crystal may be open in the interior of the crystal but they are evidently blocked at the surface since, if these channels were open, they would give rise to a concentration profile in z- rather than y-direction. However, the 10-ring channels in the "roof" section are presumably not blocked or only partially blocked. Therefore, at short times, the "roof" section fills rapidly through the 10-ring channels (in the z-direction) while at longer times we see the filling of the central cuboid section through the 8-ring channels (y-direction).

In order to simplify the quantitative analysis of the adsorption/desorption curves and of the corresponding concentration profiles the interference microscopy measurements have been carried out near the (x, y) edge of the crystal. In this case adsorption/desorption in the "roof" section is essentially of no influence for the data obtained. Representative adsorption and desorption curves for methanol on ferrierite near the crystal edge ($z = 2\,\mu$m, obtained by integrating over the profiles as presented in Fig. 1(b) in y-direction), measured over small differential pressure steps at 298 K, are shown in Figs. 2 and 3. The adsorption and desorption curves (expressed as $(m_t - m_0)/(m_\infty - m_0)$) are almost identical, suggesting that the system is essentially linear over these small concentration steps. The semi-logarithmic plots of $1 - (m_t - m_0)/(m_\infty - m_0)$ vs. t show that the uptake kinetics are well represented by the surface resistance model (Eq. (1)).

Figure 4 shows the corresponding experimental adsorption and desorption profiles in the y-direction, near the crystal edge for pressure steps $5 \rightarrow 10$ and $10 \rightarrow 5$ mbar. These profiles are compared at selected times in Fig. 5. The adsorption profiles are slightly more strongly curved than the desorption profiles but the average profiles are reasonably well represented by the theoretical profiles calculated from the dual resistance model (Eq. (6)) with the same parameter values

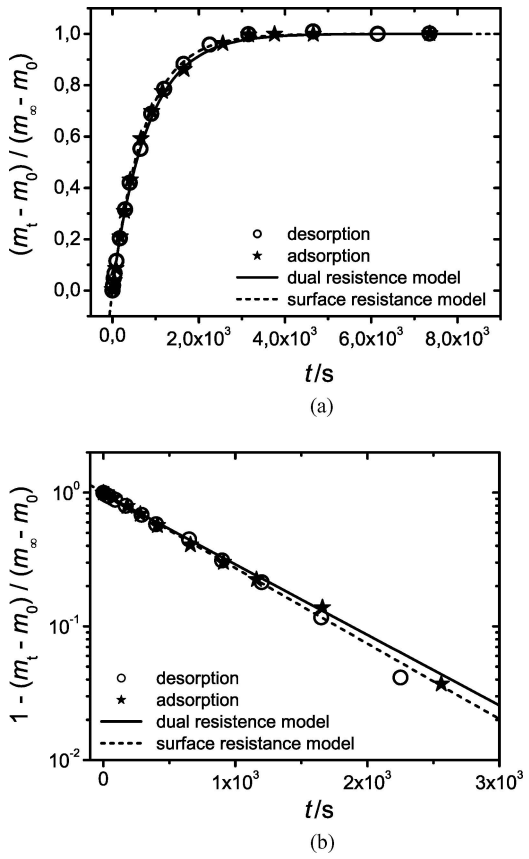

Figure 2. Experimental adsorption and desorption curves for methanol-ferrierite at 298 K measured over pressure steps 5 → 10 and 10 → 5 mbar near the crystal edge ($z = 2\,\mu$m) by the IFM technique, plotted on linear and semi-logarithmic scales. Also the theoretical curves calculated from the surface resistance model (Eq. (1)) with $\alpha/l = 1.35 \times 10^{-3}\,\mathrm{s}^{-1}$ and from the dual resistance model (Eq. (5)) with $\alpha/l = 1.68 \times 10^{-3}\,\mathrm{s}^{-1}$, $D/l^2 = 1.31 \times 10^{-3}\,\mathrm{s}^{-1}$ are shown.

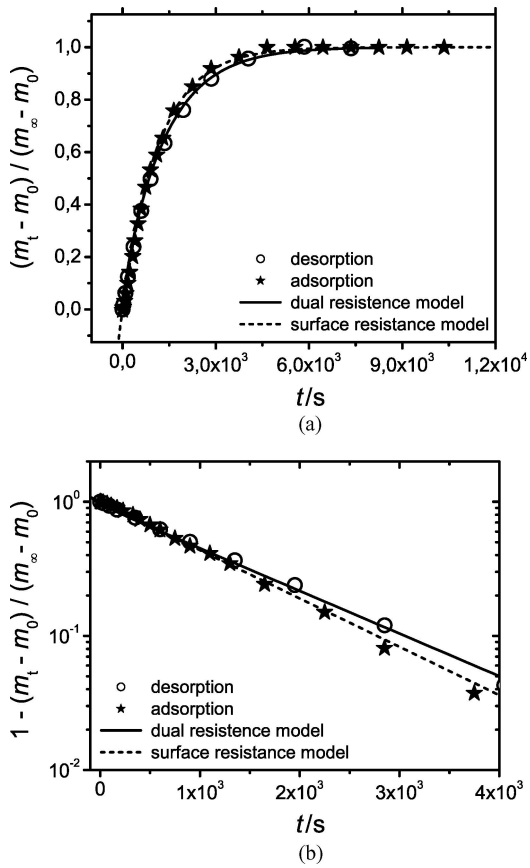

Figure 3. Experimental adsorption and desorption curves for methanol-ferrierite at 298 K measured over pressure steps 0 → 5 and 5 → 0 mbar (near the crystal edge $z = 2\,\mu$m) by the IFM technique, plotted on linear and semi-logarithmic scales. Also the theoretical curves calculated from the surface resistance model (Eq. (1)) with $\alpha/l = 8.55 \times 10^{-4}\,\mathrm{s}^{-1}$ and from the dual resistance model (Eq. (5)) with $\alpha/l = 1.60 \times 10^{-3}\,\mathrm{s}^{-1}$, $D/l^2 = 4.48 \times 10^{-4}\,\mathrm{s}^{-1}$ are shown.

($\alpha = 4.2 \times 10^{-8}\,\mathrm{ms}^{-1}$, $D = 8.1 \times 10^{-13}\,\mathrm{m}^2\,\mathrm{s}^{-1}$, $l = 25\,\mu$m). These values for α and D were established by a systematic interation and optimization procedure.

Although the overall uptake curves (Fig. 2) can be reasonably well represented by the surface resistance model (with $\alpha/l = 1.75 \times 10^{-4}\,\mathrm{s}^{-1}$) these curves are actually represented somewhat more accurately by the dual resistance model with the parameters derived from analysis of the transient concentration profiles. The actual surface rate coefficient is almost double the value estimated from the single resistance (surface control) model.

Figure 6 shows similar concentration profiles near the crystal edge for the pressure steps 0 → 5 and 5 → 0 mbar. The difference in the shapes of the adsorption and desorption profiles is much more pronounced than for the pressure steps 5 → 10 and 10 → 5 mbar. As a result, these profiles cannot be properly represented by the dual resistance model with constant values of α and D. The individual desorption profiles are well represented by this model, but the values of α and D vary strongly with time (see Fig. 7). This implies that Eq. (6) cannot be used in this case. The adsorption profiles cannot be adequately represented by this model, even when using different parameters at different times. These profiles have the form expected for a system in which the diffusivity increases strongly with loading (Ruthven, 2004).

The equilibrium isotherm, determined by using the IR absorption as a measure of loading, is shown in

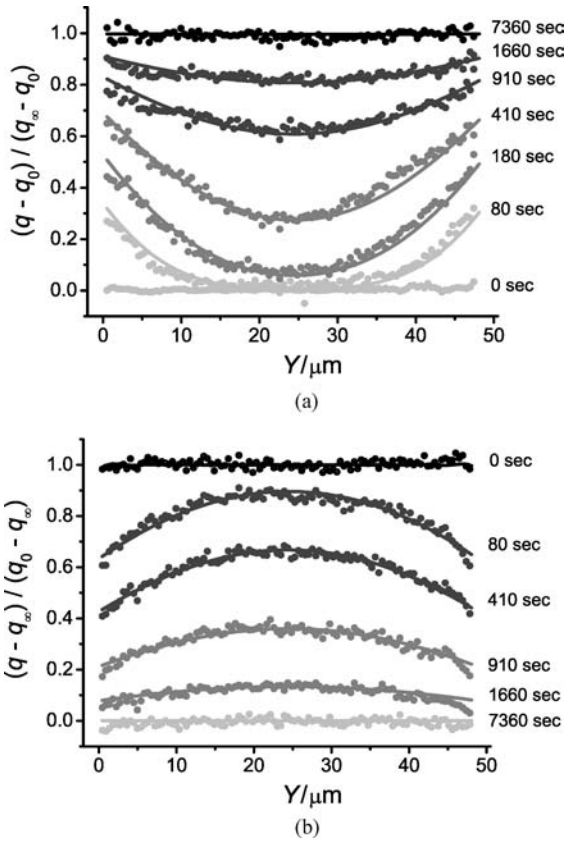

Figure 4. Experimental adsorption (a) and desorption (b) concentration profiles in the y-direction measured by interference microscopy near the edge of the crystal ($z = 2\,\mu$m) for pressure steps $5 \rightarrow 10$ and $10 \rightarrow 5$ mbar at selected times. The full lines represent the best fit of each measured profile using the dual resistance model (Eq. (6)).

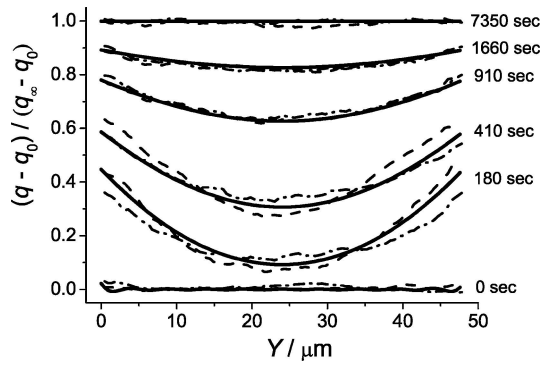

Figure 5. Comparison of adsorption (dash line) and desorption (dash-dot line) concentration profiles near the crystal edge (from Fig. 4) at selected times. Also the profiles calculated from Eq. (6) with $\alpha/l = 1.68 \times 10^{-3}\,\mathrm{s}^{-1}$, $D/l^2 = 1.31 \times 10^{-3}\,\mathrm{s}^{-1}$ (solid line) are shown.

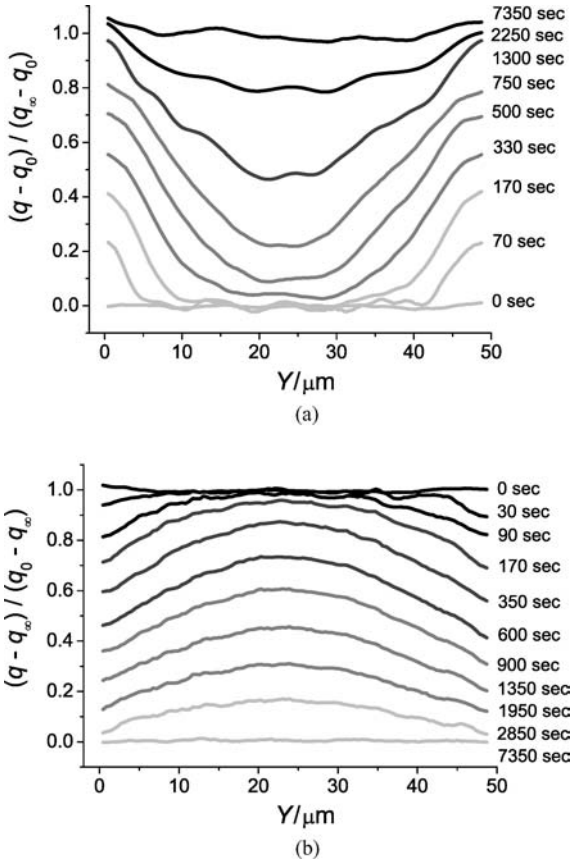

Figure 6. Experimental adsorption (a) and desorption (b) concentration profiles in the y-direction near the crystal edge ($z = 2\,\mu$m) measured by interference microscopy for pressure steps $0 \rightarrow 5$ and $5 \rightarrow 0$ mbar.

Fig. 8. Clearly at methanol pressures of less than 10 mbar the isotherm is essentially linear, so a strong concentration dependence of the diffusivity at such low loadings seems surprising. Nevertheless, that is what the data suggest.

Disguised Kinetics

For the small crystal sections near the (x, y) edge of the crystal and the small differential pressure steps $0 \rightarrow 5$ and $5 \rightarrow 10$ mbar the experimental uptake curves (Figs. 2 and 3) conform well to the surface resistance model, even though more detailed analysis shows a significant effect of internal diffusional resistance in addition to the surface barrier. Using Eq. (6) we find the following parameters for the pressure step $5 \rightarrow 10$ mbar: $D = 8.1 \times 10^{-13}\,\mathrm{m}^2\,\mathrm{s}^{-1}$, $\alpha = 4.2 \times 10^{-8}\,\mathrm{m}\,\mathrm{s}^{-1}$. At the same time, the experimental uptake curves measured by

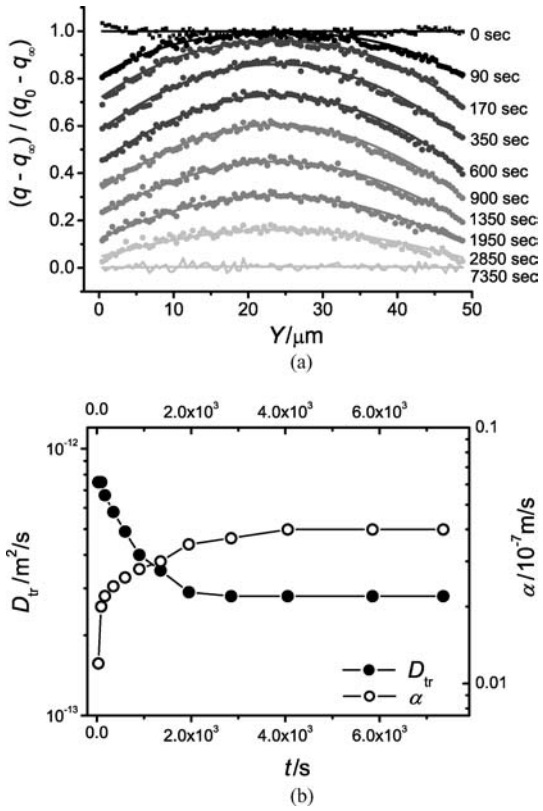

Figure 7. Matching the individual desorption profiles of Fig. 6(b) to Eq. (6) (pressure step 5 → 0 mbar) (a) and variation of the matching parameters α and D with time (b).

interference microscopy for the whole crystal and the same differential pressure steps 0 → 5 and 5 → 10 mbar (resulting from an integration over the total crystal area) are better described by the

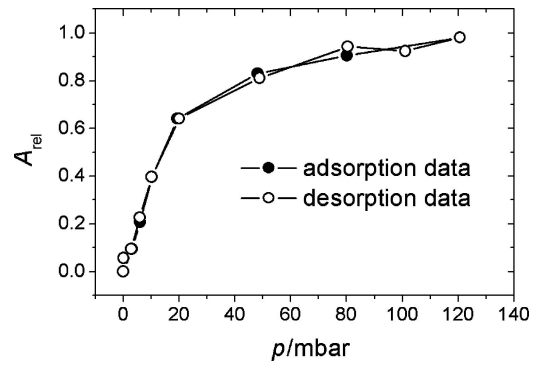

Figure 8. Equilibrium isotherm for methanol–ferrierite at 298 K plotted using IR absorbance as a measure of loading. A_{rel} is the relative loading, obtained by normalizing the data to the measured equilibrium value.

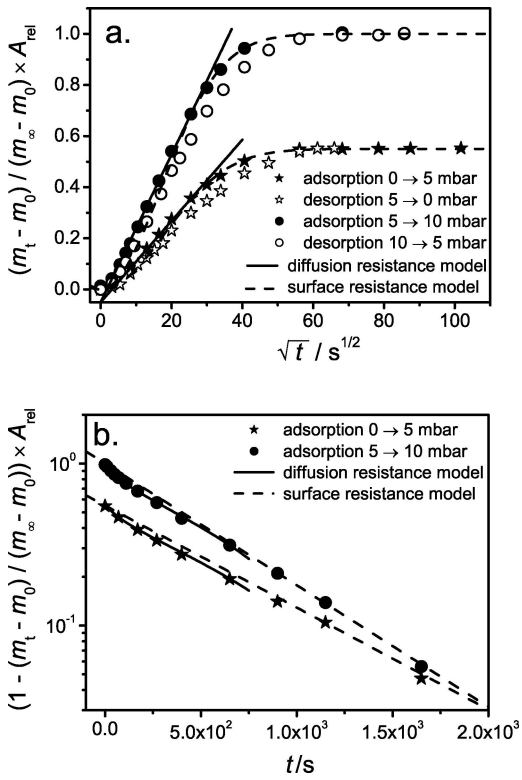

Figure 9. Experimental adsorption curves measured for the entire crystal by interference microscopy for different pressure steps. Also shown are the theoretical curves calculated from the surface resistance model (Eq. (1)) and from the diffusion resistance model (Eq. (4)). To ensure use of one presentation for both plots, the sorption curves are referred to the relative loading A_{rel} as shown in Fig. 8.

surface resistance model (Fig. 9). The apparent agreement with the diffusion model in this case is misleading. It is related to the combined influence of the two following processes: (i) the rapid adsorption/desorption in the "roof" sections of the crystals, which is mostly controlled by the intracrystalline diffusion, and (ii) the much slower adsorption/desorption in the main body of the crystal, which is controlled by the permeation of surface resistances.

Uptake curves for the whole ferrierite crystals have also been measured directly by using IR-microscopy. An example of the measured adsorption-desorption curves is shown in Fig. 10. It is seen that the discrepancy between the adsorption and desorption branches in Fig. 10 is larger in comparison with the data obtained by IFM. This large discrepancy may be attributed to the larger pressure step (0 → 10 mbar) used for the IR-microscopy measurements, which leads to a more pronounced influence of the concentration dependencies

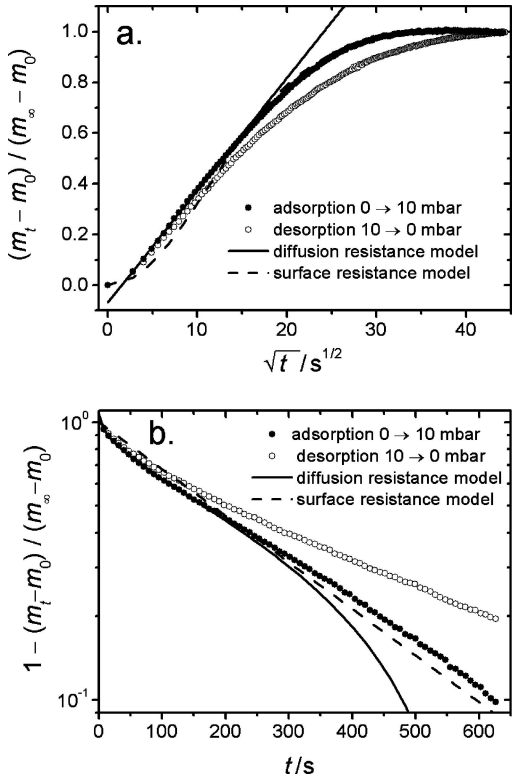

Figure 10. Experimental adsorption curves measured for the entire crystal by IR-microscopy for the pressure steps 0 → 10 and 10 → 0 mbar. Also shown are the theoretical curves calculated from the surface resistance model (Eq. (1)) and from the diffusion resistance model (Eq. (4)).

of the diffusivity and permeability of surface resistances on the uptake curves. Despite this discrepancy both curves in Fig. 10 can be reasonable well represented by the average slope in the initial region. In agreement with the IFM data, the uptake curves measured by IRM were found to conform better to the diffusion model than to the surface resistance model (Fig. 10).

If we had only the overall uptake curve we might logically choose to interpret these data according to three different models:

(a) Isotropic diffusion in an equivalent sphere with $R = 12\ \mu$m for the experiment by IFM and $R = 9.1\ \mu$m for IRM, respectively. This is the value that gives the same external surface/volume ratio as for the crystal actually used.
(b) Diffusion in the y direction ($l = 25.0\ \mu$m for IFM, $l = 15\ \mu$m for IRM)
(c) Diffusion in the z direction ($l = 112.5\ \mu$m for IFM, $l = 87.5\ \mu$m for IRM)

Table 1. Diffusivities for methanol in ferrierite and apparent diffusivities derived from uptake curves (shown in Figs. 9 and 10) measured by IF-microscopy and IR-microscopy for methanol–ferrierite, 298 K. For comparison, in the legend also literature data for other zeolites are given.

Model		D/r^2 (s^{-1})	D/l^2 (s^{-1})	D (m^{2}s^{-1})
(a) Isotropic	IFM	7.6×10^{-5}	–	1.1×10^{-14}
	IRM	1.7×10^{-4}	–	1.4×10^{-14}
(b) $D - y$	IFM	–	6.5×10^{-4}	4.1×10^{-13}
	IRM	–	1.5×10^{-3}	3.4×10^{-13}
(c) $D - z$	IFM	–	6.5×10^{-4}	8.2×10^{-12}
	IRM	–	1.4×10^{-3}	1.1×10^{-11}

Actual diffusivity (D_y) $\approx 8.1 \times 10^{-13}$ m^2 s^{-1} (5–10 mbar)
Measured differential diffusivity in NaX (low loading) D (isotropic) $= 7 \times 10^{-13}$ m^2 s^{-1} (ZLC)[14]
Measured integral diffusivity in CaA (isotropic) $= 1 \times 10^{-13}$ m^2 s^{-1} (IF-microscopy)[8].

The diffusivity values derived from these three models are shown in Table 1. Despite the larger pressure step used for the IRM measurements and the fact that the measurements by the two different techniques have been performed with different crystals, the values of the apparent diffusivities (last column) derived from the IRM data show reasonably good agreement with the values obtained from the IFM data.

It is clear that for the system considered, in which the shape of the crystal is far from equidimensional, the choice of diffusion model leads to differences of several orders of magnitude in the derived diffusivity value. Furthermore, because the apparent diffusivity derived from the uptake curve according to Eq. (4) actually reflects the combined effects of surface and internal diffusional resistances, even when the correct direction of diffusion is assumed, the derived diffusivity is much smaller than the true value. Without knowledge of the transient concentration profiles, as for conventional uptake measurements, it is most reasonable to assume that the uptake rate is primarily determined by diffusion along the largest 10-ring channels in the z-direction. This would lead to an apparent diffusivity 8.2×10^{-12} m^2 s^{-1}, which is an order of magnitude larger than the measured diffusivity in y-direction (8.1×10^{-13} m^2 s^{-1}).

Conclusions

Detailed measurements of sorption rates and transient intracrystalline concentration profiles reveal that the sorption kinetics of methanol in ferrierite are controlled

by the combined effects of surface resistance and intracrystalline diffusion, in the y-direction through the 8-ring channels. There is no measurable flux in the z-direction suggesting that access to the 10-ring channels must be blocked at the surface.

Even at low loading ($\sim$10% of saturation) the intracrystalline diffusivity appears to be strongly concentration dependent (increasing with loading) although the equilibrium isotherm is essentially linear. Similar behavior was observed previously in an experimental study of diffusion of methanol in NaX crystals by ZLC and PFG NMR methods (Bandani et al., 1995). This makes it difficult to derive reliable differential diffusivity values except from differential measurements over very small concentration steps. For the $5 \rightarrow 10$ and $10 \rightarrow 5$ mbar steps the adsorption/desorption curves and the transient concentration profiles are well represented by the combined surface resistance and one-dimensional diffusion model (Eqs. (5) and (6)).

Comparative data for diffusion of methanol in the isotropic pore systems of zeolites NaX (12-ring) and CaA (8-ring) are included in Table 1. The present diffusivity value for diffusion in the 8-ring channels of ferrierite is remarkably similar to the value obtained previously by ZLC and PFG NMR methods for diffusion in the (12-ring) channels of NaX (Grenier et al., 1994) and significantly larger than the integral values (obtained by interference microscopy) for diffusion in zeolite A (Kärger et al., 2000).

The problem of determining reliable intracrystalline diffusivities from macroscopic sorption rate measurements has been fully discussed in the literature. However, the main focus has generally been on the need to eliminate extra-crystalline resistances to heat and mass transfer and the possible intrusion of surface barrier resistance. Recent experimental studies have shown that surface resistance arising from a thin surface barrier (a region of low diffusivity close to the external surface) is quite common in zeolite crystals-see for example (Wloch, 2003). This seems to be the most reasonable physical explanation for the surface barriers observed in the present study although other explanations are also possible. The present study shows that, for non-isotropic crystals, even if all extracrystalline resistances are eliminated, uncertainties over the main direction of intracrystalline diffusion and the choice of diffusion model may still lead to large uncertainties in the diffusivity values estimated from uptake rate measurements, especially when there is also significant surface resistance.

The traditional test for diffusion control (linearity of a plot of uptake vs. the square root of time) also appears to be unreliable since a combination of surface and internal diffusion with the effect of crystal shape can evidently mimic the characteristic uptake curve for intracrystalline diffusion control.

Nomenclature

a	ratio of surface area to volume of crystal (m^{-1})
D	diffusivity ($m^2\ s^{-1}$)
l	half thickness of crystal (in y-direction) (m)
α	surface mass transfer coefficient (defined by Eq. (1))
L	parameter $\alpha \cdot l / D$
q	adsorbed phase concentration
q_0	initial value of q
q_∞	final (equilibrium) value of q
R	equivalent radius of crystal ($= 3/a$) (m)
t	time (s)

Acknowledgments

We dedicate this paper to Professor Wolfgang Schirmer on the occasion of his 85th birthday. Financial support by the Humboldt-Foundation, Deutsche Forschungsgemeinschaft (International Research Group "Diffusion in Zeolites" and International Research Training Group 1056 "Diffusion in Porous Materials"), Fonds der Chemischen Industrie and Max-Buchner-Forschungsstiftung is gratefully acknowledged.

References

Begin, van den N.G. and L.V.C. Rees, "Zeolites: Facts, Figures, Future," P.A. Jacobs and A. van Santen (Eds.), in *Proc. 8th International Zeolite Conference*, p. 915, Amsterdam, 1989.

Brandani, S., D.M. Ruthven, and J. Kärger, "Concentration Dependence of Self-Diffusivity of Methanol in NaX Zeolite Crystals," *Zeolites*, **15**, 494–496 (1995).

Crank, J., *Mathematics of Diffusion,* Oxford University Press, London, 1956.

Eic, M. and D.M. Ruthven, "Diffusion of linear paraffins and cyclohexane in NaX and 5A zeolite crystals," *Zeolites*, **8**, 472 (1988).

Geier, O., S. Vasenkov, E. Lehmann, J. Kärger, R.A. Rakoczy, and J. Weitkamp, "Interference Microscopy as a Tool of Choice for Investigating the Role of Crystal Morphology in Diffusion Studies," *J. Phys. Chem. B,* **105**, 10217–10222 (2001).

Grenier, Ph., F. Meunier, P.G. Gray, J. Kärger, Z. Xu, and D.M. Ruthven, "Diffusion of Methanol in NaX Crystals: Comparison

of IR, ZLC, and PFG NMR Measurements," *Zeolites*, **14**, 242–249 (1994).

Hermann, M., W. Niessen, and H.G. Karge, "Sorption kinetics of *n*-Hexane in MFI-type Zeolites Investigated by Micro-FTIR Spectroscopy," *Stud. Surf. Sci. Catal.,* **94**, 131–138 (1995).

Kärger, J. and J. Caro, "Interpretation and Correlation of Zeolitic Diffusivities Obtained from Nuclear Magnetic Resonance and Sorption Experiments," *J. Chem. Soc. Faraday Trans. I*, **73**, 1363 (1977).

Kärger, J., H. Pfeifer, and M. Bülow, "Untersuchung der Adsorpt-Selbstdiffusion auf Zeolithen mit Hilfe der NMR-Feldgradientenimpulstechnik," *Z. Chemie*, **16**, 85–90 (1976).

Kärger, J., U. Schemmert, and S. Vasenkov, "Adsorption Science and Technology," in *Proc. 2nd Pacific Conference On Adsorption*, pp. 324–328, World Scientific, Singapore, D.D. Do (Ed.), 2000.

Meier, W.M. and D.H. Olson, *Atlas of Zeolite Structure Types,* p. 98, Third Edition, Butterworth-Heinemann, London, 1992.

Ruthven, D.M., "Sorption Kinetics for Diffusion-Controlled Systems with a Strongly Concentration-Dependent Diffusivity," *Chem. Eng. Sci.*, **59**, 4531–4545 (2004).

Schirmer, W., G. Fiedrich, A. Grossmann, and H. Stach, *Proc. 1st International Zeolite Conference*, London (1967), *Soc. Chem. Ind.*, London, pp. 276–288 1968.

Wloch, J., "Effect of Surface Etching of ZSM-5 Zeolite Crystals on the Rate of *n*-Hexane Sorption," *Microporous and Mesoporous Mater.,* **62**, 81–86 (2003).

Yasuda, Y., "Determination of Vapour Diffusion Coefficients in Zeolite by the Frequency Response Method," *J. Phys. Chem.,* **86**, 1913 (1982).